JOURNAL OF GEOPHYSICAL RESEARCH, VOL. 114, B00A14, doi:10.1029/2008JB006040, 2009

A search in strainmeter data for slow slip associated with triggered and ambient tremor near Parkfield, California

Emily F. Smith[1] and Joan Gomberg[1]

Received 27 August 2008; revised 15 February 2009; accepted 19 August 2009; published 1 December 2009.

[1] We test the hypothesis that, as in subduction zones, slow slip facilitates triggered and ambient tremor in the transform boundary setting of California. Our study builds on the study of Peng et al. (2009) of triggered and ambient tremor near Parkfield, California during time intervals surrounding 31, potentially triggering, $M \geq 7.5$ teleseismic earthquakes; waves from 10 of these triggered tremor and 29 occurred in periods of ambient tremor activity. We look for transient slow slip during 3-month windows that include 11 of these triggering and nontriggering teleseisms, using continuous strain data recorded on two borehole Gladwin tensor strainmeters (GTSM) located within the distribution of tremor epicenters. We model the GTSM data assuming only tidal and "drift" signals are present and find no detectable slow slip, either ongoing when the teleseismic waves passed or triggered by them. We infer a conservative detection threshold of about 5 nanostrain for abrupt changes and about twice this for slowly evolving signals. This could be lowered slightly by adding analyses of other data types, modeled slow slip signals, and GTSM data calibration. Detection of slow slip also depends on the slipping fault's location and size, which we describe in terms of equivalent earthquake moment magnitude, M. In the best case of the GTSM above a very shallow slipping fault, detectable slip events must exceed $M\sim2$, and if the slow slip is beneath the seismogenic zone (below $\sim$15 km depth), even $M\sim5$ events are likely to remain hidden.

Citation: Smith, E. F., and J. Gomberg (2009), A search in strainmeter data for slow slip associated with triggered and ambient tremor near Parkfield, California, *J. Geophys. Res.*, *114*, B00A14, doi:10.1029/2008JB006040.

1. Introduction

[2] This study tests observationally the hypothesis that, as in subduction zones [e.g., *Rogers and Dragert*, 2003; *Schwartz and Rokosky*, 2007; *Ide et al.*, 2008; *Rubinstein et al.*, 2009; *Brudzinski*, 2008], slow slip also accompanies tremor in the transform boundary setting of California. Herein slow slip refers to a transient increase in the slip rate of a fault patch that otherwise creeps steadily or is locked. This transient slip is sufficiently slow that no appreciable seismic energy is radiated, and it lasts for minutes to days. We test this hypothesis that slow slip accompanies triggered tremor using direct measurements of strain with the greatest potential resolution; i.e., using continuous strain signals recorded on borehole Gladwin tensor strainmeters (GTSM) [*Gladwin*, 1984] operated along the Parkfield section of the San Andreas fault in California (Figure 1).

[3] A second intent of this paper is to provide basic guidance to others planning to use, or to assess the potential of, the newly available GTSM data from the numerous installations that comprise part of the Plate Boundary Observatory in the western United States. In addition to addressing the aforementioned scientific question, we sought to explore what first-order information could be learned from strainmeter data by nonexperts. In our opinion, a deterrent to using strainmeter data is the challenge of removing the noise (signals of nontectonic origin), which often is larger than the signal of interest. More sophisticated analyses than our approach typically involve modeling of theoretical tidal loading using programs like BAYTAP [*Tamura et al.*, 1991] and of the statistical properties of the remaining noise [see *Langbein*, 2004, and references therein]. While a more sophisticated analysis likely would have improved the resolution of our results, the gain did not clearly seem to justify the significantly increased effort, particularly given our scientific objectives. This seemed further justified given some of the large data uncertainties and the modifications needed to the more sophisticated analyses to accommodate some of the data shortcomings (e.g., uneven data sampling and gaps), We focused exclusively in this study on the GTSM data, but if it is revisited, other types of relevant data (e.g., dilatometers) from the same region could be included.

1.1. Why Parkfield?

[4] In some subduction zones there is clear association between slow slip and ambient tremor and a growing number of observations that indicate that slow slip facilitates triggered tremor [*Rogers and Dragert*, 2003; *Ide et al.*, 2008; *Rubinstein et al.*, 2009]. Several published studies lead us to suggest that triggered tremor may serve as a proxy for slow slip [*Peng et al.*, 2009; *Rubinstein et al.*, 2009]. Such a proxy

[1]U.S. Geological Survey, Department of Earth and Space Sciences, University of Washington, Seattle, Washington, USA.

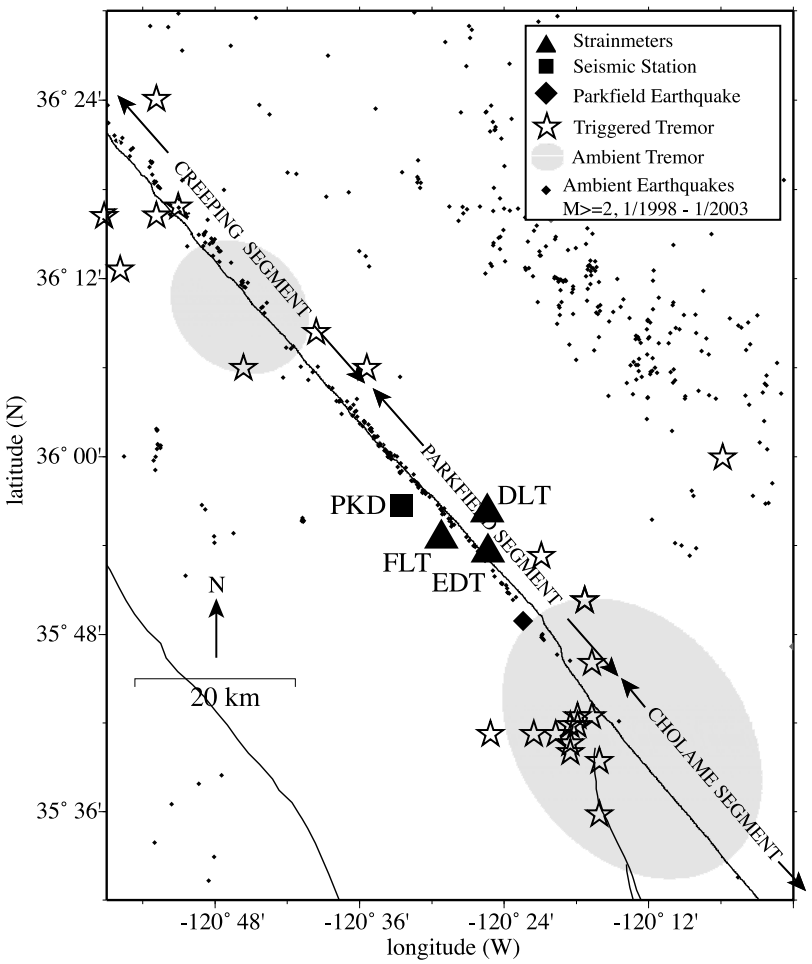

Figure 1. Map of Parkfield and adjacent segments of the San Andreas fault (curved lines), showing regions of ambient tremor (shaded ovals; from R. Nadeau (personal communication, 2008)) and tremor sources (stars; locations from *Peng et al.* [2009]) triggered by 10 teleseismic earthquakes. Triangles show the GTSM instrument locations (FLT, DLT, EDT corresponding to the Frolich, Donna Lee, and Eades sites), the broadband seismic station PKD (square) used in the triggered tremor observations, the epicenter of the 2004 M6 Parkfield earthquake (larger diamond) and background seismicity (small diamonds).

would have the potential benefit of being much more widely observable than slow slip given the abundance of locations with triggered seismic recording stations relative to sites that record continuous seismic or slow deformation (e.g., have strainmeters, GPS, tiltmeters).

[5] In addition to subduction zones, clear evidence of both ambient and triggered tremor exists in the transform boundary in California, in the vicinity of the Parkfield section of the San Andreas fault (Figure 1) [*Nadeau and Dolenc*, 2005; *Gomberg et al.*, 2008; *Peng et al.*, 2009]. The first observation of triggered tremor at Parkfield was that triggered by the M7.9 Denali, Alaska earthquake [*Rubinstein et al.*, 2007]. Of particular relevance to this study, *Peng et al.* [2009] examined seismograms of 31 teleseismic earthquakes with $M \geq 7.5$ at stations near Parkfield, California and found clear evidence of tremor triggered by waves from 10 of these. While there is a clear correlation between triggered tremor and triggering wave amplitude the imperfectness of the correlation implies the triggering probability depends on other factors as well. We propose and test the hypothesis that, as in subduction zones, slow slip may facilitate tremor generation and thus may be observed during times of triggered and ambient tremor near Parkfield. Answering this question is key to understanding whether the tremor observed outside subduction zones results from the same processes as within, or if there are multiple causes possibly unique to the local environment.

[6] The Parkfield region is a particularly well suited place to test our hypothesis because the location and properties of the faults are among the most well constrained in the world. In addition, there is an abundance of instruments to measure both slow slip and tremor, along the Parkfield and adjacent sections of the San Andreas. The GTSM and other similar instruments in California were installed in the mid-1980s with a primary goal of detecting deformation changes of the order of a few nanostrain that might be precursory to damaging earthquakes [*Johnston et al.*, 1992] and to record the anticipated M6 "Parkfield" earthquake [*Johnston et al.*, 2006]. We focus on data from the Parkfield GTSM instruments because of their proximity to the triggered tremor sources (Figure 1 and *Peng et al.* [2009]), their >20 year duration of operation (e.g., start-up transients should be

Table 1. Earthquake Information[a]

Earthquake	Date	Time (LT)	Magnitude	Maximum Velocity (cm/s)	Distance of Earthquake to Parkfield (km)	Tremor
Peru	23 Jun 2001	2033:14.130	8.40	0.0593	7593.93	Yes
Denali	23Oct 2002	1127:18.000	6.70	0.0055	3598.73	No
Denali	3Nov 2002	2212:41.518	7.90	0.3880	3572.95	Yes
Hokkaido	25 Sep 2003	1950:06.360	8.30	0.0532	7867.99	Yes
Macquarie	23 Dec 2004	1459:04.410	8.10	0.0615	12167.03	No
Sumatra	26 Dec 2004	0058:53.450	9.10	0.0862	14249.11	Yes
Nias	28 Mar 2005	1609:36.530	8.70	0.0291	14275.68	No
Mendocino	15 Jun 2005	0250:54.190	7.20	0.0222	757.54	Yes
Tonga	3 May 2006	1526:40.290	8.00	0.0459	8384.42	Yes
Kurile	15 Nov 2006	1114:13.570	8.30	0.0492	6959.48	Yes
Kurile	13 Jan 2007	0423:21.010	8.10	0.1440	6886.77	Yes

[a]Origin time, moment magnitude, measured maximum velocity at broadband station PKD, (Figure 1), source-receiver distance and flag indicating whether tremor was triggered. These are only a subset of the 30 teleseismic waves examined for triggered tremor by *Peng et al.* [2009].

negligible and calibrations should be well determined), and their potential to record the complete strainfield (i.e., all components of the surface strain tensor).

1.2. Hypotheses and Strategy

[7] We seek to answer the question of whether slow slip accompanies triggered tremor using the GTSM data for time periods surrounding the arrival of potentially triggering waves. Separation of the observed strains that are due to nontectonic sources from those potentially due to slow slip requires modeling. Effectively we ask if we can model the GTSM data assuming they reflect only nontectonic sources, with a negative answer indicating signals of possible tectonic origin. A positive answer or equivalently, failure to reject this null hypothesis, still provides useful constraints on the detection threshold and thus bounds on the geometry and magnitude of slow slip that the tremor cannot be attributed to (see section 3).

[8] We pose two versions of the above hypothesis. The first considers the possibility that the San Andreas or other nearby faults were already slipping when the teleseismic waves arrived. The second considers the possibility that the waves themselves cause the fault to begin to slip as well as produce tremor. This seems possible given previous observations of slow slip preceded by earthquakes in the San Juan Bautista section of the San Andreas, just north of Parkfield [*Pollitz and Johnston*, 2006]. Additionally, slow slip events were likely triggered by seismic waves on southern California faults [*McGill et al.*, 1989; *Glowacka et al.*, 2002], and seismic waves have triggered seismic slip in a number of locations [*Hill and Prejean*, 2007]. Based on the duration of slow slip events documented previously along the San Andreas (see section 1.3) and in subduction zones, we look for slow slip events as clear strain changes that become apparent over fractions of days to a few days and lasting several to tens of days or more. The detection threshold should be lower if we know the expected onset time, which in the case of the second version of the hypothesis, corresponds to the arrival time of the seismic waves.

[9] In the remainder of this Introduction, we summarize previous strainmeter observations of slow slip along the San Andreas and elsewhere. In section 2 we describe our approach to processing strain data from GTSM instruments near Parkfield for time periods surrounding the arrival of teleseismic waves that did and did not trigger tremor in the Parkfield region (Figure 1 and Table 1) [*Peng et al.*, 2009]. Effectively, we assess the detection capabilities of these data. In section 3 we interpret the results in terms of slow fault slip, by comparing estimated detection thresholds to theoretical strain fields computed for a range of plausible scenarios. A discussion and conclusions are presented in section 4.

1.3. Previous Observations of Slow Slip Along the San Andreas Fault System

[10] Herein we summarize some of the features of slow slip and its signature in strainmeter data noted previously along the transform boundary San Andreas fault system in central California. We do so in order to demonstrate the reasonableness of our hypothesis and to serve as a guide as to what signals to look for in the Parkfield GTSM data.

[11] Slow slip events have been documented in the Parkfield and San Juan Batista sections of the San Andreas fault system on a variety of geodetic instruments, as well as on other central California faults [*Bilham and Whitehead*, 1997; *Galehouse and Lienkaemper*, 2003] and on faults in southern California [*Bilham*, 1989; *Bilham et al.*, 2004]. Changes in strain rate lasting years, punctuated by episodic more abrupt deformation (days to months) have been documented in the Parkfield GTSM data, electronic distance meter measurements, and sometimes in creepmeter data as well [*Langbein et al.*, 1999; see also information at http://www.gtsmtechnologies.com/index_files/advfaqs.htm]. Just to the north of the creeping section (Figure 1), along the San Juan Bautista section, a sequence of slow slip events lasting about a week in 1992 was documented on several types of strainmeters along the with clearly correlative changes in seismicity rates and creep [*Linde et al.*, 1996]. This sequence produced unambiguous signals of a microstrain or more, and modeling indicates the slip occurred in the upper 4 km of the fault with equivalent magnitudes of 4.8 [*Linde et al.*, 1996]. *Pollitz and Johnston* [2006] examined seismicity following this sequence and 3 other M$\sim$5 slow slip events on the San Juan Bautista section (in 1996, 2003, and 2004), recorded on strainmeters. Modeling of strainmeter, GPS, and InSAR data that include these slow slip events indicate they occurred in the upper 5–8 km of the fault where it also slips steadily [*Johanson and Bürgmann*, 2005].

[12] We consider the possibility that slow slip may occur at nearly any depth within the crust. The slow slip events in the above cases, as well as steady slip or creep on other faults in the region (where often temporal resolution is insufficient to resolve rapid ''events'', if they occur [*Schmidt et al.*, 2005; *Funning et al.*, 2007]) have been modeled as occurring at or above seismogenic depths (e.g., above about $\sim$10 km) [*Linde*

et al., 1996; *Johanson and Bürgmann*, 2005]. The same frictional models developed to explain this shallow slow slip or creep have also been proposed to explain slow slip below the locked portion of subduction zones where slow slip and tremor likely originates [*Marone and Scholz*, 1988; *Boatwright and Cocco*, 1996; *Liu and Rice*, 2007]. While the conditions at shallow depths, above the seismogenic or locked zone, and those below this zone clearly differ, they both may lead to similar frictional behaviors. The sediments above the seismogenic or locked zone and the high temperatures below both can be described by similar frictional properties and behaviors that lead to slow slip.

2. Data Analyses

[13] Our goal is to use two of the Parkfield GTSM strain data to determine if nearby faults are slipping during, or as a consequence of, the passage of the seismic waves that trigger tremor. We do so by attempting to reject a null hypothesis that no detectable slow slip is occurring. This section describes the process we have employed to test our hypothesis and estimate the detection limits of the GTSM data. This process is simpler, but similar to processes used previously, such as those implemented in widely used software package program "BAYTAP" [*Tamura et al.*, 1991], and most recently for "level 2" data provided by the Plate Boundary Observatory (PBO) facility for newer GTSM instruments (see http://pboweb.unavco.org/?pageid=89).

2.1. Processing Methodology

[14] The GTSM instruments are designed to measure strain at a resolution of better than a nanostrain to the period range 0.01 s to years [*Gladwin*, 1984; *Gladwin and Hart*, 1985]. The range of detection capabilities of strainmeters provides constraints on slow and wave-triggered permanent deformation that are theoretically unobtainable using seismometers or GPS. The strainmeters are installed in the bottom of boreholes, several hundred meters below the Earth's surface and measure deformation of the surrounding rock using extensometers that respond to the relative displacement of its anchor points. The GTSMs' nominal high level of sensitivity of ~0.3 nanostrain [*Johnston et al.*, 1987] is what makes the instrument so important and useful, but also complicates the process of separating tectonic from nontectonic (noise) signals. The latter includes changes in atmospheric pressure, wind turbulence, pore pressure, groundwater motion, and earth tides and a frequency-dependent sensitivity to these [*Agnew*, 1986].

[15] The basic measurement is the horizontal extension, u_i, of three or four gages mounted inside the borehole at different azimuths, approximately 120° apart. Although a general strain tensor has six components, at the surface plane stress equations prevail (the vertical stresses are zero) and only three horizontal strains are needed to fully characterize the deformation. To describe the deformation more meaningfully, these gage measurements are used to estimate the strains, ε_{EE}, ε_{EN}, ε_{NN}, measured in a geographic coordinate system. Alternatively, the deformation can be described by the areal strain, $A = \varepsilon_{EE} + \varepsilon_{NN}$, the differential extension, $\gamma_1 = \varepsilon_{EE} - \varepsilon_{NN}$, and the shear, $\gamma_2 = 2\varepsilon_{EN}$. This is particularly convenient for studying deformation along the San Andreas because γ_1 and γ_2 represent pure engineering shear strains that are maxima across planes oriented NW–SE and NE–SW or roughly parallel to the San Andreas fault, and N–S and E–W, respectively.

[16] For the Parkfield strainmeters, one can obtain either the gage measurements nominally corrected to strain units, or areal and shear strains measurements. The relationship between the gage measurements, u_i, and the areal and shear strains is [*Hart et al.*, 1996]

$$\begin{bmatrix} u_1 \\ u_2 \\ u_3 \end{bmatrix} = \begin{bmatrix} \frac{1}{g_1} & 0 & 0 \\ 0 & \frac{1}{g_2} & 0 \\ 0 & 0 & \frac{1}{g_3} \end{bmatrix} \begin{bmatrix} \frac{1}{2} & \frac{1}{2}\cos(2\theta_1) & \frac{1}{2}\sin(2\theta_1) \\ \frac{1}{2} & \frac{1}{2}\cos(2\theta_2) & \frac{1}{2}\sin(2\theta_2) \\ \frac{1}{2} & \frac{1}{2}\cos(2\theta_3) & \frac{1}{2}\sin(2\theta_3) \end{bmatrix} \cdot \begin{bmatrix} c & 0 & 0 \\ 0 & d & 0 \\ 0 & 0 & d \end{bmatrix} \begin{bmatrix} t_{11} & t_{12} & t_{13} \\ t_{21} & t_{22} & t_{23} \\ t_{31} & t_{32} & t_{33} \end{bmatrix} \begin{bmatrix} A \\ \gamma_1 \\ \gamma_2 \end{bmatrix} \quad (1)$$

Θ_i is the gage azimuth, "weight", g_i accounts for mechanical differences among the gages, c and d quantify the coupling of the instrument deformation to that of the surrounding rock and parameters t_{ij} characterize the effect of topography and geology. We use resolved strain data, A, γ_1, and γ_2, obtained from the GTSM company website (http://www.gtsmtechnologies.com). We do so because we want to compare signals from different sites and the gages may have different orientations. In addition, calibration of the parameters in equation (1) using the usual procedure of calibrating with theoretical tidal loading signals is beyond the scope of this study. *Johnston et al.* [2006] suggest that calibrations of the Parkfield GTSM are repeatable to within 5%.

[17] Our analysis approach is very similar, albeit less rigorous, to that underlying the program BAYTAP [e.g., *Tamura et al.*, 1991]. In particular, BAYTAP selects the tidal components and assesses the fit to theoretical tidal models according to a Bayesian Information Criteria rather than our more qualitative approach. However, interpretation of the BAYTAP output requires an understanding of tidal and statistical modeling that seemed beyond the scope of this study (nor were we comfortable using it as a black box). In addition, in its standard form BAYTAP requires data sampled evenly at 1 h, with gaps flagged a priori. The GTSM data are sampled at 18 and 30 min at the Donna Lee and Frolich sites, respectively, with a sample missed every three hours in the data recorded at the Donna Lee site. Also, irregular gaps of a single sample to hours exist in the data from both sites. Instead of interpolating and resampling the data, and identifying all the gaps manually, our approach uses the data as recorded. Finally, we justify our approach by noting that it is more conservative because we are likely to err on the side of removing real signal with the noise rather than retaining noise that might be mistaken as tectonic signal.

[18] Following *Tamura et al.* [1991], we assume that the measured strain (which here may refer to any component), $u(t)$, as a function of time, t, may be modeled a sum of the response to (1) the tides, $\tau(t)$, (2) atmospheric pressure changes or other measured "auxiliary" loads, $a(t)$, (3) possibly some tectonic process such as a transient slow slip event, $e(t)$, (4) "drift", $d(t)$, and (5) the remaining unmodeled signal or

Table 2. Modeled Tidal Frequencies

	Tidal Component					
	O1	M2	S1	S2	Q1	N2
Period (hours)	25.8193	12.4206	24.000	12.000	26.8684	12.6583
Frequency (cyles/d)	0.929537	1.93227	1.0000	2.0000	0.893243	1.89599

residual signal, $r(t)$. Drift refers to signals of presumed nontectonic origin with periods longer those of the tides, with specific origin and precise character that is not generally known [*Tamura et al.*, 1991]. We also include the response to long-term steady tectonic loading in the drift. Thus, the measured strain is

$$u(t) = e(t) + \tau(t) + d(t) + a(t) + r(t) \tag{2}$$

The Parkfield GTSM strainmeters are relatively insensitive to atmospheric pressure changes (E. Roeloffs et al., Draft review of borehole strainmeter data collected by the U.S. Geological Survey, 1985–2004, prepared for PBO, 2004) so that $a(t) \sim 0$. The ideal null hypothesis is that the fault is not slipping, which could be tested by fitting $u(t)$ under the assumption that $e(t) = 0$ and employing parameterized models of $\tau(t)$ and $d(t)$. The residual between the modeled and observed signals becomes

$$r(t) = u(t) - [\tau(t) + d(t)] \tag{3}$$

Residual signals that by some measure, exceed the long-term variability in the differences (unmodeled stationary "noise") and also are observed on multiple components and at multiple nearby sites, would cause us to consider rejecting our hypothesis that no detectable slow slip is occurring.

[19] We model the tidal signal, $\tau(t)$, as a sum of N sine waves with periods, T_n, and solve for the amplitude, S_n, and phase, ϕ_n, of each that maximizes the fit to the data. We choose the minimum number of periods required to fit the tidal signals, expected to dominate at Parkfield (Table 2), and so that the frequency spacing was not smaller than the inverse of the time series length (i.e., only fit resolvable variations in frequency). The tidal fitting process becomes linear using the identity

$$\begin{aligned} S_n \sin(\omega_n t + \phi_n) &= C_n \sin(\omega_n t) D_n \cos(\omega_n t), \\ S_n = \sqrt{C_n^2 + D_n^2}, \phi_n &= \tan^{-1}\left(\frac{C_n}{D_n}\right), \omega_n = \frac{2\pi}{T_n} \end{aligned} \tag{4}$$

The data are sampled at M discrete time points, t_m, so our tidal signal model may be written as

$$\tau(t_m) = \sum_{n=1}^{N} [C_n \sin(\omega_n t_m) + D_n \cos(\omega_n t_m)] \tag{5}$$

[20] Since we have no physical model of the drift, $d(t)$, we use the same approach as *Tamura et al.* [1991], parameterizing it as a time series sampled at the same time points as the data and constrained to be "smooth". This constraint is imposed by taking the second derivative of $d(t)$ numerically and equating it to a "data" vector of zeroes. For evenly sampled time points, the numerical derivative at t_{m+1} is simply proportional to $d(t_{m+2}) - 2d(t_{m+1}) + d(t_m)$. However, we use the more complete form that includes the sample interval because unlike many other applications and more recently installed strainmeters, the Parkfield data are not evenly sampled and have gaps, and we wish to retain the maximum temporal resolution to look for strain changes on the timescale of the teleseismic waves. If a sample interval is $\delta_m = t_{m+1} - t_m$, the second derivative in this case is

$$\frac{d^2 d(t_{m+1})}{dt^2} \approx 2\frac{\delta_{m+1} d(t_m) - [\delta_m + \delta_{m+1}] d(t_{m+1}) + \delta_m d(t_{m+2})}{\left[\delta_m \delta_{m+1}^2 + \delta_{m+1} \delta_m^2\right]} \tag{6}$$

To test the hypothesis that the data reflect only the response to the tides and drift, we solve the linear equations

$$\begin{aligned} u(t_m) &= \tau(t_m) + d(t_m) \\ &= \sum_{n=1}^{N} [C_n \sin(\omega_n t_m) + D_n \cos(\omega_n t_m)] + d(t_m) \qquad m = 1, M \end{aligned} \tag{7}$$

with the constraint that

$$\begin{aligned} 0 &\approx 2\frac{\delta_{m+1} d(t_m) - [\delta_m + \delta_{m+1}] d(t_{m+1}) + \delta_m d(t_{m+2})}{\left[\delta_m \delta_{m+1}^2 + \delta_{m+1} \delta_m^2\right]} \\ m &= 1, M-2 \end{aligned} \tag{8}$$

These can be written in matrix form and solved using least squares or some other method. The matrix equation to solve is

$$\begin{bmatrix} u(t_1) \\ u(t_2) \\ \cdots \\ u(t_M) \\ 0 \\ 0 \\ \cdots \\ 0 \end{bmatrix} = \begin{bmatrix} TidalMatrix & IdentityMatrix \\ ZeroMatrix & K * DerivativeMatrix \end{bmatrix} \begin{bmatrix} C_1 \\ D_1 \\ C_2 \\ \cdots \\ D_N \\ d(t_1) \\ d(t_2) \\ \cdots \\ d(t_M) \end{bmatrix} \tag{9}$$

The "data" vector contains the M observed strain values and $M - 2$ zeros corresponding to the constraint on the drift derivatives. Our unknowns are the $2N$ weights corresponding to the N tidal frequencies and M values of the drift at each time point. The smoothness of the drift is controlled by the scaling factor K; i.e., larger values result in smoother drift time series and a poorer fit to the observed strain values. We choose this factor subjectively, noting that even though more formal processing approaches such as BAYTAP find the

optimal value, the final choice of K is a user adjustable parameter. We chose values that produced drift signals that varied on time scales longer that the slow slip signals we were looking for. Each row of the $M \times 2N$ (number of rows and columns, respectively) tidal matrix corresponds to the datum at the mth time point and contains paired terms $\sin(\omega_n t_m)$ and $\cos(\omega_n t_m)$ $n = 1,N$ corresponding to each tidal frequency. The derivative matrix is banded such that each row corresponds to the second derivative at t_{m+1} and contains three consecutive nonzero elements weighting the unknown drift values $d(t_m)$, $d(t_{m+1})$, $d(t_{m+2})$ in equation (8). The identity and zero matrices have dimensions $M \times M$ and $(M-2) \times 2N$, respectively.

2.2. Application to the Parkfield Gladwin Tensor Strainmeter Data

[21] Availability of Gladwin Tensor Strainmeter (GTSM) strainmeter data varies from instrument to instrument due to occasional instrument malfunctions. We analyzed GTSM data from the Donna Lee and Frolich sites (Figure 1) for time periods surrounding 11 of the teleseismic earthquakes analyzed by *Peng et al.* [2009] between 2001 and 2007 and listed in Table 1. Based on the duration of slow slip events observed previously at Parkfield (section 1.3) and to robustly estimate drift, we examined data from 2 months prior to and 1 month after each earthquake. The GTSM data from the third Parkfield site (Eades) were not included because the instrument failed in 2002 so that data are available for only one of the eleven events.

[22] Our analysis strategy involved analyzing each strain component, the shear ($\gamma_1$and γ_2) and areal (A) strains, independently fitting tidal and drift models, $\tau(t)$ and $d(t)$, to each using the formulation described in the previous section and finding a least squares solution. For each time period we compared the raw and modeled time series at the Donna Lee and Frolich sites to assess the accuracy of the data, appropriateness of our assumptions, and to identify signals indicative of slow slip events. Comparison of the observed and modeled (as a superposition of fit sine waves of specified frequencies (equation (5)) tidal signals for the same strain component at the two sites provide a measure of the accuracy of the calibrations and stability of the responses. Drift signals that are not coherent between the two sites indicate we are not erroneously including tectonically driven signal in $d(t)$. Finally, amplitude deviations in residual strains (observed minus modeled strains) that exceed the long-term variability must do so at both the Donna Lee and Frolich sites to be considered of possible tectonic origin. We show examples of observed and modeled strains for strain components for the data surrounding the 2002 M7.9 Denali, Alaska and 2006, M8.0 Tonga earthquakes in Figures 2 and 3, respectively, with residual strains for all other data analyzed provided in the auxiliary material.[1] We include Figure 3 because the data highlight the need for analyses that can account for data gaps; this is a somewhat extreme example but nearly all the time windows examined have time gaps of some duration.

[23] Based on our visual inspections we found no evidence of slow slip larger than the long-term variability in the residual strains and that correlates between like components of either the drift or the residual signals at the Donna Lee and Frolich sites, or of slow slip induced by the passage of the teleseismic waves.

2.2.1. Noise and Accuracy

[24] Having data from two sites within ~7 km of one another proved useful for assessing the accuracy of the estimated strains and thus, because we do not observe any tectonic signals, the detection limits of deformation associated with slow slip. In addition to visual inspection of the observed and modeled time series, we identify systematic differences and quantify the variability among all the measurements for the three different strain components at the Donna Lee and Frolich sites using a simple metric of the RMS signal value. This somewhat ad hoc approach does not explicitly account for the fact that the noise and detection threshold depend on the time interval considered [*Langbein*, 2004, and references therein], but nonetheless reveals some significant uncertainties in the calibrations, temporal changes in noise levels, and provides constraints on detection thresholds. For example, a lower detection threshold for time windows of hours to a few days, relative to that for many days, is clearly evident in simple visual comparisons of the residual signals plotted for the entire 3 month windows and six day windows (see Figures 2 and 3 and Figures S1–S6 in the auxiliary material).

[25] We first present evidence that the calibrations (sensitivities or conversions from instrumental measurement to strain) are uncertain by a factor of ~2, although we cannot determine which strainmeter is incorrect. Differences in the observed and modeled tidal signals at the Donna Lee and Frolich sites provide this evidence, because the tidal loads should be identical at both sites. Without any processing it is clear that the peak-to-peak tidal amplitudes of the γ_1 and γ_2 strains are consistently larger at the Frolich site. A more quantitative assessment comes from the ratios of the RMS tidal signals at the two sites; although the tidal signals are time varying, ratios between signals from the two sites should be unity. Such ratios clearly show that prior to 2006, relative to the Donna Lee site, the strains at the Frolich site are smaller by 82% for the areal strains and 200% larger for the γ_1 and γ_2 strains (Figure 4b). We focus on observations prior to 2006 for reasons discussed below.

[26] Perhaps more troubling than these differences in sensitivities is an apparent time-varying difference in the tidal phase response between the sites. In most cases the tidal signals in the Donna Lee and Frolich data appear to be in-phase (e.g., Figures 2a and 2d), but this is not always true (Figure 5). Examination of one case in which the mismatch is significant shows that the phase difference does not arise abruptly or during a data gap, as one might expect if some instrument parameter was reset or the timing system failed suddenly. As shown in Figure 5, we speculate that the mismatch arises because the frequency response is not properly calibrated. In other words, the tidal signal is a sum of semidiurnal and diurnal tides that appear to have different amplitudes at the two sites, so that the peaks of the summed signal sometimes appear out of phase. Additional environmental or instrumental noise in the tidal frequency band might exacerbate this mismatch. An alternative explanation might be that the timing system drifted at one or both sites.

[1] Auxiliary materials are available in the HTML. doi:10.1029/2008JB006040.

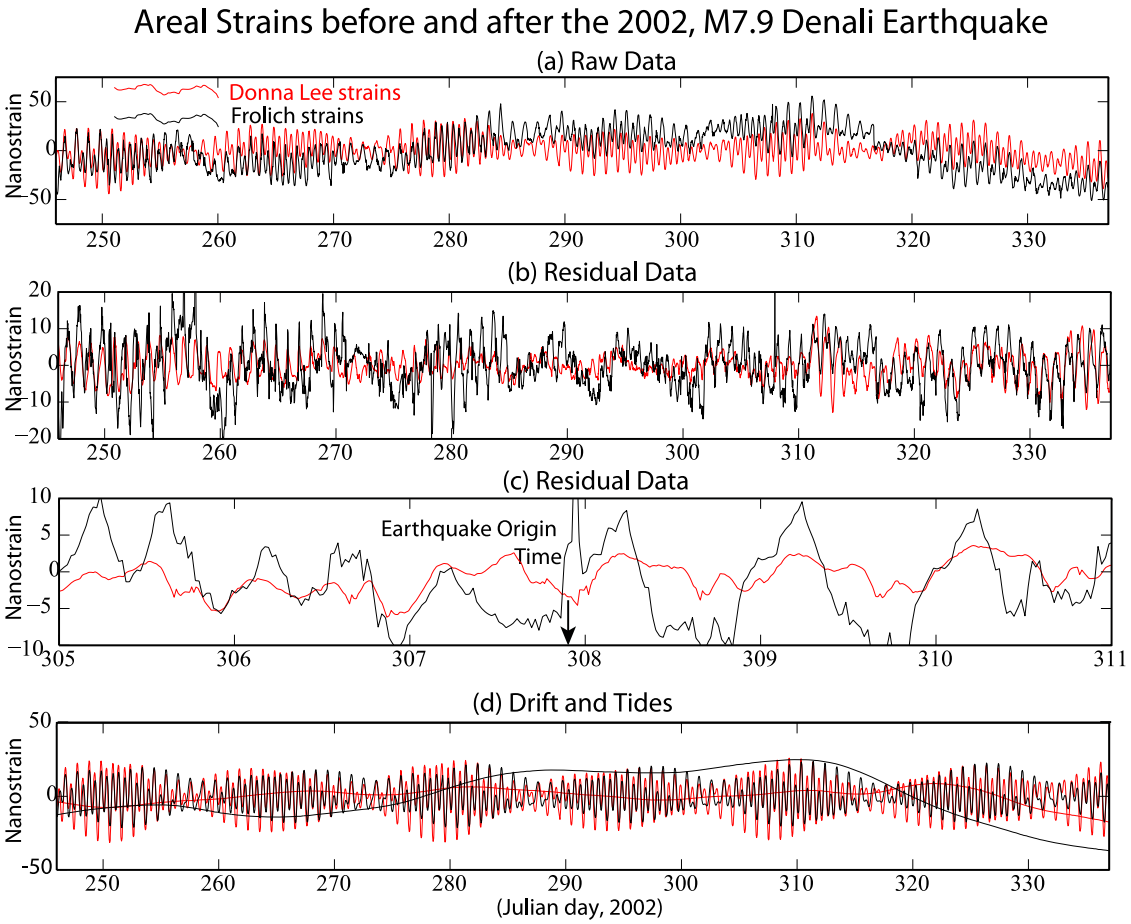

Figure 2. Areal strains recorded at the Donna Lee (red) and Frolich (black) GTSM sites. (a) Strains with only the trend and mean offset removed. (b) Strains in Figure 2a minus the modeled drift and tidal signals in Figure 2d. (c) Expanded view of the strains 3 days before and after the arrival of the Denali waves. The large peak just prior to day 308 is the transient deformation associated with the Denali surface waves. (d) Modeled tidal and drift signals.

[27] We next consider the residual signals and what they reveal about the instrument performance and detection threshold. Visual inspection of data for the two Kuril Island earthquakes in 2006 and 2007 (see the auxiliary material) and RMS tidal and residual amplitudes (Figure 4) indicate significant changes in the responses at both sites for these events. Independently, a more quantitative analysis of the performance of Frolich station that compared the theoretically predicted and observed tidal phases revealed a clear deterioration in gage 2 of the Frolich strainmeter starting in 2006 (J. Langbein, personal communication, 2008). In addition, the RMS residuals from the Frolich site suggest its response, or noise levels changed markedly at several times during the study period. Figure 4c shows stable average RMS residual values for Donna Lee site for all but the 2006 and 2007 Kuril earthquakes of 1.3, 2.0, and 3.8 nanostrain for the γ_1, γ_2, and areal strains, respectively. The RMS residuals for the Frolich γ_2 and areal strains appear to fall into at least two groups; from 2001 to 2003 we measure values of 6.5 and 7.3 nanostrain respectively, and from 2004 to 2006 values for both increase to 12.8 nanostrain. The Frolich γ_1 RMS residual strains remain stable over the entire period with an average value of 4.8 nanostrain. If we consider these time periods, the standard deviations of all these averages are less than a few nanostrains.

[28] The apparent sensitivity differences estimated from the tidal strains (e.g., Frolich γ_1 and γ_2 signals being twice those at Donna Lee) cannot account for differences in RMS residuals at the two sites, even during the quieter 2001–2003 period. Thus, we infer that the noise levels of the data from the Frolich site are about twice those recorded at the Donna Lee site. Our inference is not consistent with spectral analyses of hourly data by E. Roeloffs et al. (draft review, 2004) that indicate roughly equal signal-to-noise ratios for data from the Frolich and Donna Lee sites. We suggest that some of the difference in results may be due to the fact that we are looking at higher frequencies and have done much less averaging.

[29] The largest amplitude signals we observe generally are the drift, with average values of several tens of nanostrain but with significant variability, sometimes exceeding 100 nanostrain. The drift has periods of tens of days or more usually does not correlate between the strainmeters (Figures 2d and 3d). Some of this drift may reflect localized hydrologic changes, which seems plausible considering the strainmeters are on opposite sides of the San Andreas fault. For example, E. Roeloffs et al. (draft review, 2004) show

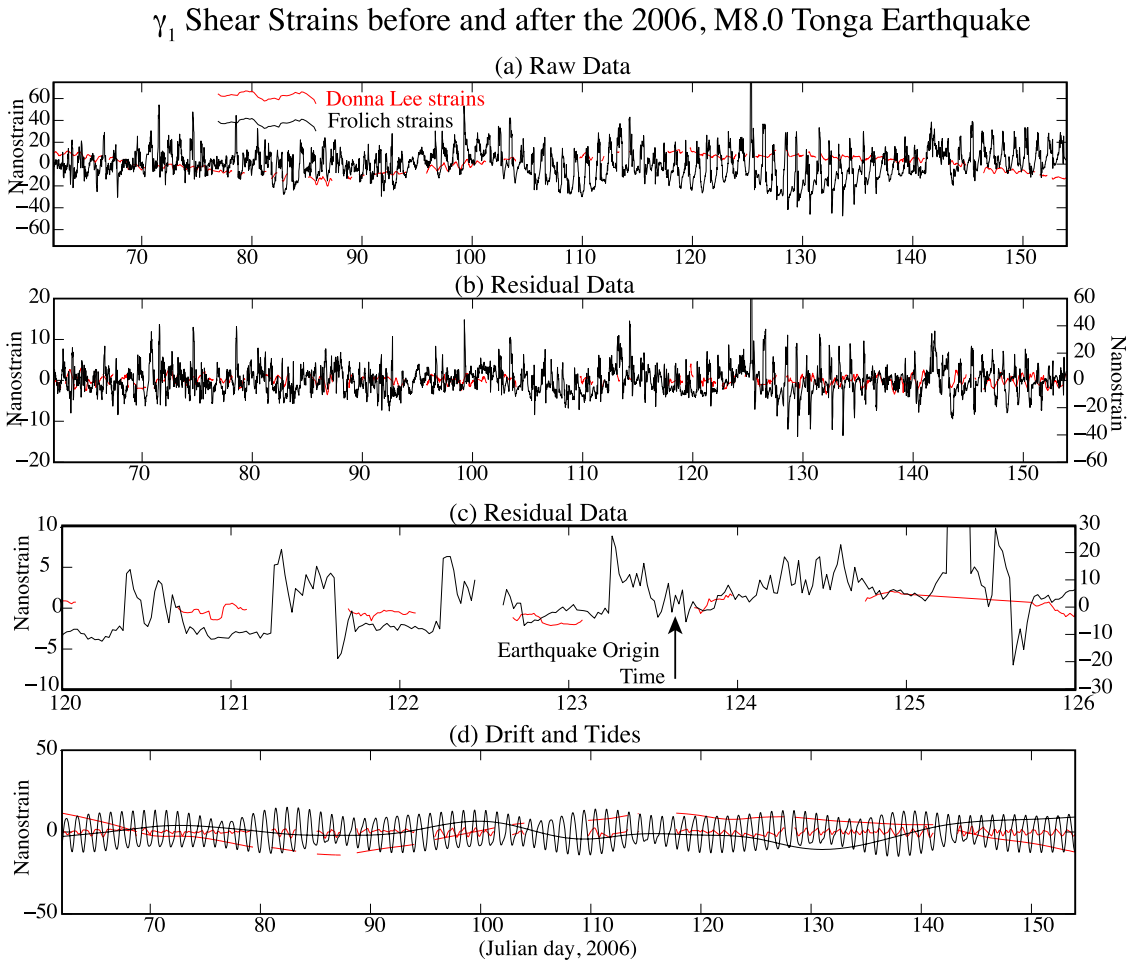

Figure 3. The γ_1 shear strains recorded at the Donna Lee (red) and Frolich (black) GTSM sites. This strain component represents a differential extension; i.e., $\gamma_1 = \varepsilon_{EE} - \varepsilon_{NN}$. (a) Strains with only the trend and mean offset removed. See text for explanation. (b) Strains in Figure 3a minus the modeled drift and tidal signals in Figure 3d. Note that the amplitude scales for the Donna Lee (left axis) and Frolich (right axis) data differ in this plot and for Figure 3c. (c) Expanded view of the strains 3 days before and after the arrival of the Tonga earthquake waves. The waves arrive on day 123 but are not resolvable in these data. (d) Modeled tidal and drift signals.

that GTSM data from 1993 to 1997 at the Donna Lee site are contaminated by a hydrological signal caused by a nearby unconfined aquifer, which does not affect signals at the Frolich site.

2.2.2. Short-Term and Long-Term Strains

[30] If our hypothesis that no detectable tectonic deformation occurred during the time windows examined is true, the residual strains on time scales of slow slip ("long term") and wave-triggered deformation ("short term") should (1) be independent of the magnitude of the waves, (2) show no signals larger than the long-term variability and (3) be incoherent at both the Donna Lee and Frolich sites. We find these three criteria to be satisfied for all eleven time periods containing teleseismic waves examined. These strains provide a bound on the detectability of any slow slip signal; i.e., any slow slip signals would go undetected if they evolved over days and were smaller than the long-term residual strains or were induced by the waves themselves and were smaller than the short-term residual strains. Based on the results of the previous section we estimate the long-term detection threshold at the quieter (Donna Lee) site is approximately 10 nanostrain. This conservatively accounts for the factor of two uncertainty in calibration by assuming that the Donna Lee strains are underestimated by this amount and adds a standard deviation to the largest average RMS residual measured for the three strains. Based on visual comparison of the short-term and long-term residual plots (Figures 2, 3, and S1–S6) we estimate a detection threshold for wave-induced slow slip of approximately half the long-term value, or about 5 nanostrain.

3. Implications for Slow Slip Detection

[31] To interpret the detection thresholds of the GTSM data in terms of detectable fault slip we modeled the expected strain using a three-dimensional dislocation model [*Okada*, 1992; *Gomberg and Ellis*, 1994], and calculated the horizontal surface shear strain that would result from slip along a vertical strike-slip fault. We varied the fault depth, dimensions, and slip (Figure 6 and Table 3), and we constrained the slip to be purely strike slip in keeping with the dominant mode of faulting in the region. The thresholds we infer must

be viewed only as guides to the detectability of slow slip because these static models only provide constraint on the total deformation change expected for the specified slip, without regard to its time history. For example, the detection threshold might be lowered by searching for signals that match theoretical models of the temporal evolution of a slow slip signal.

[32] The calculated strain scales linearly with the assumed value of the slip, so that any increases or decreases in the latter would simply scale the strain signal proportionally. We assign slip values and refer to slip event sizes based on the scaling expected if the slip occurred coseismically as in an earthquake. Earthquake size may be described by its seismic moment

$$M_o = \mu DLW \tag{10}$$

and its moment magnitude

$$M = 2/3 \log M_o - 6.07 \tag{11}$$

μ is the shear modulus ($\sim 3 \times 10^4$ MPa), D is the average slip, L and W are the rupture length and width, respectively [*Hanks and Kanamori*, 1979], and M_o has units of N m. The commonly used empirical relations of *Wells and Coppersmith* [1994] between parameters L, W, D, and M provide constraints on the ratio of slip to rupture dimensions. For example, their relations for strike-slip faults imply that

$$D = L^{1.45} 10^{-4.54} \tag{12}$$

with D in cm and L in km. Another constraint comes from the relation between stress drop, $\Delta\sigma$, D and rupture dimensions, that

$$\Delta\sigma \sim \mu D/(LW)^{1/2} \tag{13}$$

Typical values of $\Delta\sigma$ range between 1 and 10 MPa with significant scatter (see *Kanamori and Brodsky* [2004] for a summary), suggesting ratio of slip to rupture dimension of 3×10^{-5} to 3×10^{-4}. This is slightly greater than values implied by the *Wells and Coppersmith* [1994] relations so we choose a value of 10^{-5}, which is a compromise and is consistent with the suggestion that tremor and slow slip sources are low stress drop events [*Ide et al.*, 2008].

[33] We plot our inferred detection thresholds with the modeled surface shear strain calculated along profiles at distance 0.25 km from the surface trace of the faults and striking parallel to them (Figure 6). This shows that the ability to detect a strain signal depends strongly on the GTSM's location relative to the slipping fault, the size of the fault, and

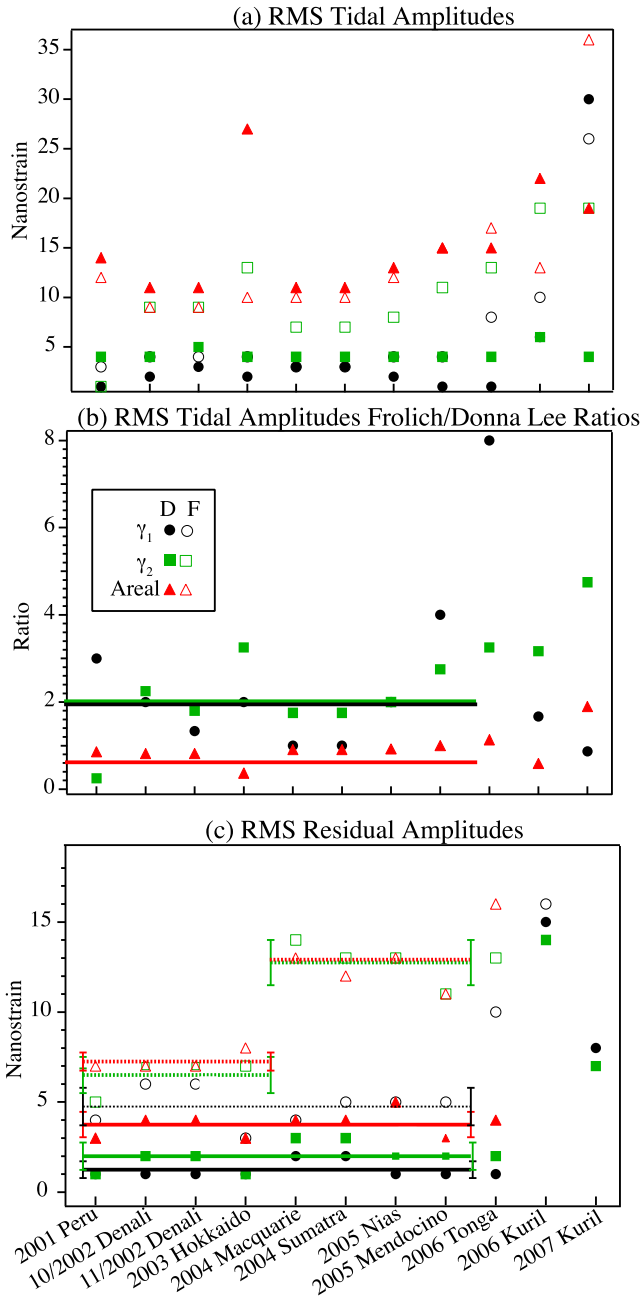

Figure 4. To identify systematic differences or dependencies on wave characteristics, and to quantify the variability among all the measurements of the γ_1 (circles), γ_2 (squares), and A (triangles) strain components at the Donna Lee (solid symbols) and Frolich (open symbols) sites we plot the RMS values for the time series corresponding to each earthquake (bottom axis, Table 1). The time windows span 3 months, centered on the arrival times of waves from each earthquake. (a) RMS modeled tidal signals show that the Frolich γ_1 and γ_2 strains are systematically larger than those at Donna Lee. All but the Donna Lee γ_2 strains appear anomalously large for the Kuril earthquakes. (b) Ratios of the observations in Figure 4a (Frolich/Donna Lee) clearly show that on average the Frolich γ_1 and γ_2 strains are twice those at Donna Lee and smaller for the areal strains. Horizontal lines indicate mean values of the corresponding, color-coded strain component, excluding the suspect measurements starting in 2006 (Donna Lee data for the 2006 Tonga event have a tremendous number of gaps, although the estimates for them appear consistent with the others). (c) RMS values for the residual strains with mean and ±1 standard deviation values shown by the horizontal lines and error bars, respectively. The Frolich estimates prior to 2006 seem to cluster in two groups; both suggest a higher noise level at the Frolich site that increases significantly after 2003.

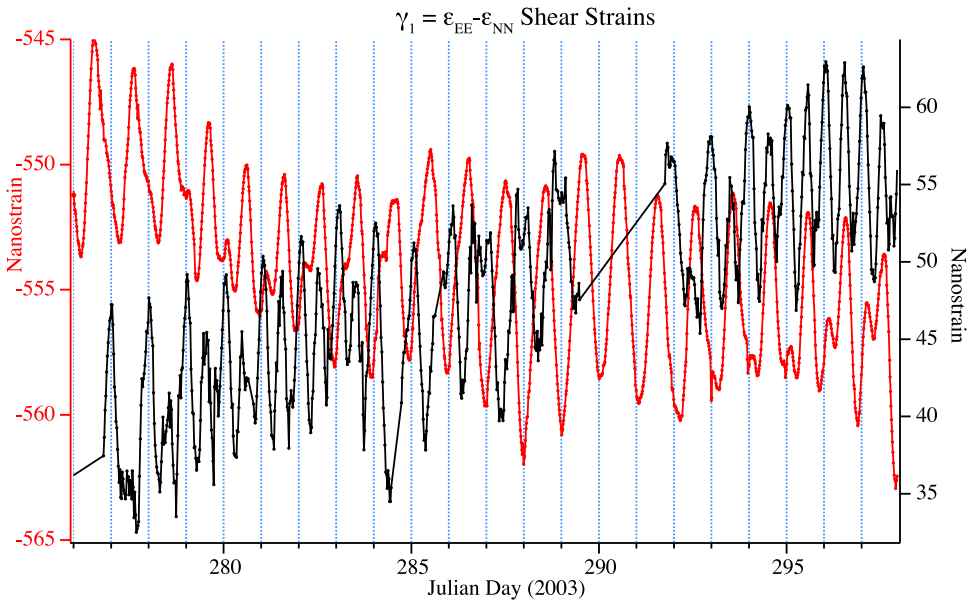

Figure 5. The $\gamma_1 = \varepsilon_{EE} - \varepsilon_{NN}$ shear strains from the Donna Lee (red) and Frolich (black) sites for the time period surrounding the 2003 Hokkaido earthquake. Sample points are shown by dots; nominal sampling rates are 18 and 30 min for the Donna Lee and Frolich sites, respectively. Irregular gaps of a single sample to several days exist in the Frolich data, and a sample is missed every 3 hours in the Donna Lee data. Note the relative phasing (i.e., relative timing of peaks or troughs at the two sites) appears to vary over even a few days. This may be due in part to differing sensitivities to the semidiurnal tides and contamination by noise sources with periods in the tidal band.

its depth. If one is immediately atop a very shallow fault, the magnitude of the strain decreases by nearly four orders of magnitude as the slip event decreases from M∼5 to M∼1. Even in this most optimal situation, the smallest event above the detection threshold of the GTSM instruments has M∼3 (LW∼0.25 km^2, D∼5 mm). The strains also decrease rapidly with distance from the center of the fault, although more gradually as its depth increases. Even at 5 km from the fault center, the models suggest that only a M∼4 or greater slip event would produce a detectable signal and, if in the center of the seismogenic zone at ∼7.5 km, this limit increases to M∼5 events. If the slow slip is beneath the seismogenic zone, the most likely depth range of the tremor [*Peng et al.*, 2009], even M∼5 events are likely to remain hidden below the noise of the GTSM instruments.

4. Discussion and Conclusions

[34] The detection threshold values we obtain, ∼10 and ∼5 nanostrain for long-term and short-term residual strains, respectively, are comparable to the values reported by *Johnston et al.* [2006], who studied deformation associated with the 2004 M6 Parkfield earthquake using data from a variety of instruments in the region. Their long-term values may be roughly consistent with ours recalling that we have conservatively allowed for the apparent calibration uncertainty and noise differences between the Frolich and Donna Lee sites (i.e., we chose the largest possible noise level). *Johnston et al.* [2006] show residual strains that vary by about 10 nanostrain at the Donna Lee GTSM site for the week prior to the earthquake, but do not show residuals the Frolich site because they exceeded their 10 nanostrain "noise" level. Their coesismic detection threshold of fractions of a nanostrain is based on nearby high-sample rate (1 s) dilatometer data, and so we cannot directly compare these to ours. Our higher threshold values may also reflect the fact that we do not use the atmospheric pressure data in our analyses, although the lack of sensitivity of the GTSM at Parkfield suggests this should not be a significant omission. Our interpretation of the threshold in terms of the maximum slow slip event that could go undetected is consistent with *Johnston et al.*'s [2006] inference that threshold of 0.01 nanostrain would correspond to an event at 8 km depth with moment 2×10^{12} N m. Thus, a threshold of ∼10 nanostrain would imply a moment of 2×10^{15} N m or a M∼4.1 (equation (11)), which agrees with results displayed in Figure 6.

[35] Another relevant study of the detection threshold focused on deformation precursory to known earthquakes, assuming the precursory slip occurred on the same fault patch that ultimately failed in the earthquakes [*Johnston et al.*, 1987]. They consider time scales of minutes, estimate a detection threshold of a few nanostrain, and by scaling coseismic offsets observed for real earthquakes suggest the smallest detectable event at 2.7 km depth and 3.2 km from the strainmeter would have M∼2.1. The most distant detectable events, at ∼56 km hypocentral distance, would have M∼4.7. These are roughly consistent with the modeled deformation in Figure 6, and our slightly more conservative inference that a 10–18 nanostrain threshold that if deeper than 15 km, only events with M > ∼5.0 may be detected.

[36] It is interesting to consider the relative potential of GPS and strainmeter data. *Langbein et al.* [2006] made such a comparison by analyzing the wealth of deformation data temporally and spatially surrounding the M6.0 2004 Parkfield earthquake. They report variability in GPS displace-

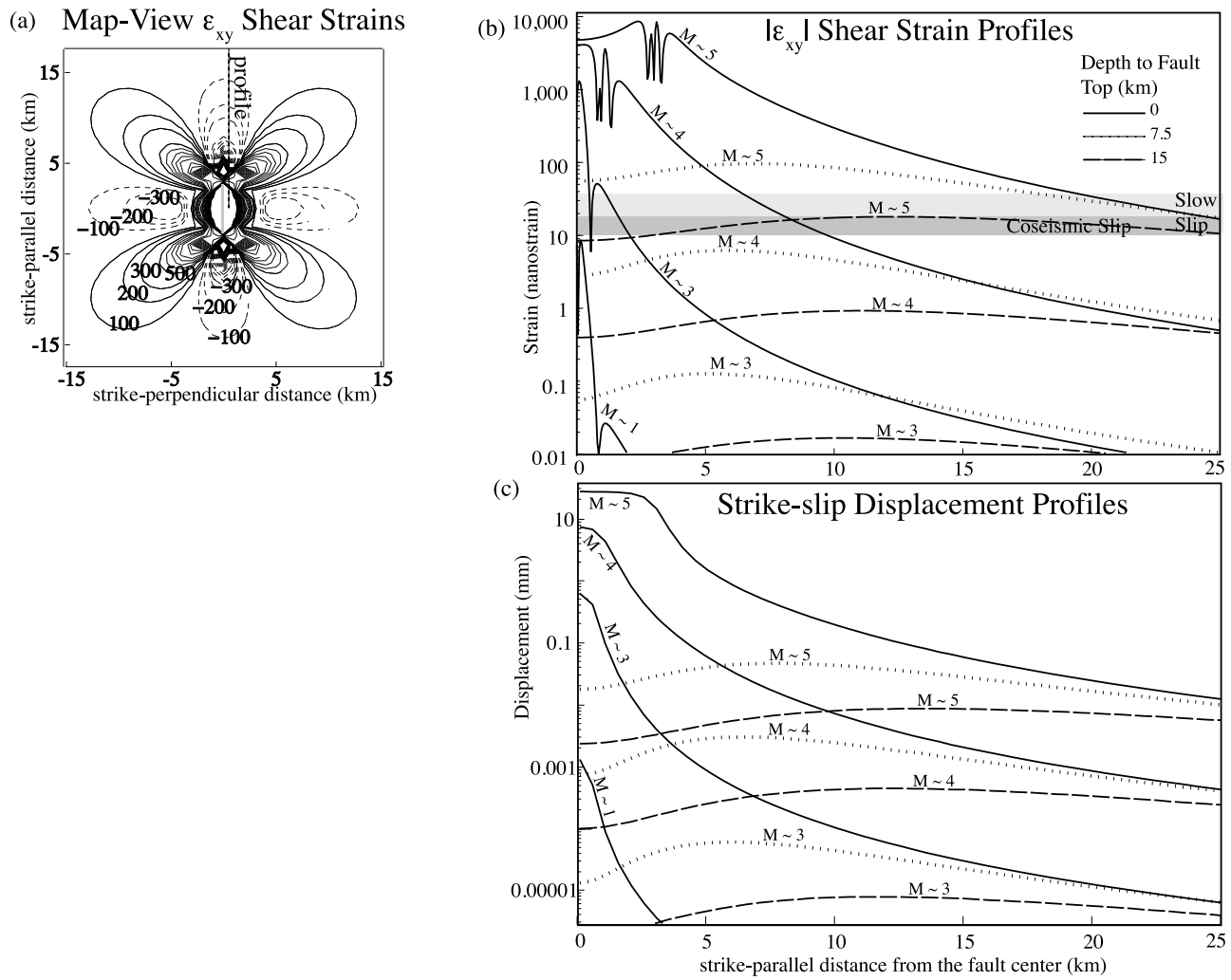

Figure 6. Predicted xy (x and y perpendicular and parallel to the fault strike, respectively) surface shear strains. (a) Contoured example of strains calculated for vertical, 36 km^2 square fault with its top edge (gray vertical line in the plot center) at the surface of the Earth with slip corresponding to a ∼M5 earthquake (Table 3). Solid and dashed lines indicate positive and negative values. (b) Absolute values of the surface shear strains along a profile located parallel to and 0.25 km offset from the fault, calculated for four sizes of slip events, each at three different depths. The darker shaded region marks the lower boundary for detection capacities for a short time frame (due to wave-triggered slip) and the lighter shaded region marks a longer time frame (due to ongoing slow slip). Even the short-term slip lower limit suggests that in order to be able to measure the strain, the GTSMs must be located in very close proximity to the fault, the fault must be very large, and/or the fault must be shallow. (c) Same as Figure 6b but showing the displacements in the strike direction.

ments (measured relative to some smoothed modeled values) that depends on the sample rate and signal duration but ranges between a fraction of a millimeter to ∼15 mm for processed measurements at high sample rate (1 Hz) lasting minutes to daily solutions, respectively (e.g., see Langbein et al.'s Figure 2). This is consistent with the results of *Titus et al.* [2006]. In Figure 6c we compare this range to the theoretical displacements calculated for the same sources as the strains in Figure 6b and infer that even given our conservative strain thresholds, the strainmeters have significantly better detection capabilities. For example, we infer that a M∼5 at 7.5 km depth should be easily observed in the strainmeter data but produces a displacement that is nearly an order of magnitude below the threshold of GPS data. It is important to note however, that such conclusions depend on the temporal nature of the signal and the particular case considered; for example, *Langbein et al.* [2006] suggest that at least in their study, which may represent somewhat of a best case for GPS

Table 3. Fault Model Dimensions, Along-Strike Slip, and Approximate Magnitude if the Slip Was Relaxed Seismically[a]

Size of Fault (km^2)	Slip (cm)	Approximate Magnitude
6 × 6	6	5
2 × 2	2	4
0.5 × 0.5	0.5	3
0.05 × 0.05	0.05	1

[a]We computed the strain fields at the surface for these four models, keeping the dip vertical and for differing depths of the top of 0.0, 7.5, and 15 km.

data, the long-term precision is much better for the GPS than the strain data, in part because the GTSM strainmeter data may suffer at this time from sensitivity to fluctuations in the water table.

[37] We find no evidence of slow slip during or as a result of the passage of tremor triggering seismic waves, or of waves that did not trigger tremor. Theoretical models show the detection threshold depends strongly on the proximity of the slip to the strainmeter, and the closest tremor source to the Parkfield GTSM sites is at an epicentral distance of ~20 km and likely below the seismogenic layer [*Peng et al.*, 2009]. If the slow slip is colocated or nearby the tremor, we are lead to the unfortunate conclusion that we can only rule out very large slip events, with equivalent M~5 or greater. This difficulty in detecting deep slip has been noted previously [e.g., see *Harris and Arrowsmith*, 2006, and references therein]. Even if not colocated with the tremor and very shallow, the smallest detectable slow slip event would still need to have an equivalent M~2 and be fortuitously located within a few km of the strainmeter. Previously studies have shown that the San Andreas fault properties permit slow slip events at shallow depths (see section 1.3), so that our failure to find evidence of slow slip may indicate that it either does not accompany the tremor or it is deep and below the detection threshold. Future work could lower the detection threshold by perhaps an order of magnitude, by recalibrating the raw data and including additional data (e.g., the atmospheric pressure or dilatometer data). However, ultimately we are limited by the fact that we can only make measurements on or very near the Earth's surface, of processes that likely occur km below.

[38] **Acknowledgments.** The authors thank Evelyn Roeloffs, Duncan Agnew, John Langbein, Wendy McCausland, and Zhigang Peng for many useful discussions and reviews. We also thank Evelyn Roeloffs, Duncan Agnew, and Kathleen Hodgkinson for teaching an extremely useful class in strainmeter data processing and UNAVCO for supporting Emily Smith's participation in the class. Finally, we acknowledge the USGS/NAGT internship program, particularly Robert Ridky.

References

Agnew, D. C. (1986), Strainmeters and tiltmeters, *Rev. Geophys.*, *24*(3), 579–624, doi:10.1029/RG024i003p00579.

Bilham, R. (1989), Surface slip subsequent to the 24 November 1987 Superstition Hills, California, earthquake monitored by digital creepmeters, *Bull. Seismol. Soc. Am.*, *79*, 424–450.

Bilham, R., and S. Whitehead (1997), Subsurface creep on the Hayward fault, Fremont, California, *Geophys. Res. Lett.*, *24*, 1307–1310, doi:10.1029/97GL01244.

Bilham, R., N. Suszek, and S. Pinkey (2004), California creepmeters, *Seismol. Res. Lett.*, *75*, 481–492, doi:10.1785/gssrl.75.4.481.

Boatwright, J., and M. Cocco (1996), Frictional constraints on crustal faulting, *J. Geophys. Res.*, *101*, 13,895–13,909, doi:10.1029/96JB00405.

Brudzinski, M. R. (2008), Do faults shimmy before they shake?, *Nat. Geosci.*, *1*, 295–296, doi:10.1038/ngeo196.

Funning, G. J., R. Burgmann, A. Ferretti, F. Novali, and A. Fumagalli (2007), Creep on the Rodgers Creek fault, northern San Francisco Bay area from a 10 year PS-InSAR dataset, *Geophys. Res. Lett.*, *34*, L19306, doi:10.1029/2007GL030836.

Galehouse, J. S., and J. J. Lienkaemper (2003), Inferences drawn from two decades of alignment array measurements of creep on faults in the San Francisco Bay region, *Bull. Seismol. Soc. Am.*, *93*, 2415–2433, doi:10.1785/0120020226.

Gladwin, M. T. (1984), High precision multi-component borehole deformation monitoring, *Rev. Sci. Instrum.*, *55*, 2011–2016, doi:10.1063/1.1137704.

Gladwin, M. T., and R. Hart (1985), Design parameters for borehole strain instrumentation, *Pure Appl. Geophys.*, *123*, 59–80, doi:10.1007/BF00877049.

Glowacka, E., F. A. Nava, G. D. deCossio, V. Wong, and F. Farfan (2002), Fault slip, seismicity, and deformation in Mexicali Valley, Baja California, Mexico, after the M7.1 1999 Hector Mine earthquake, *Bull. Seismol. Soc. Am.*, *92*, 1290–1299, doi:10.1785/0120000911.

Gomberg, J. S., and M. A. Ellis (1994), Topography and tectonics of the central New Madrid Seismic Zone: Results of numerical experiments using a three-dimensional boundary element program, *J. Geophys. Res.*, *99*, 20,299–20,310, doi:10.1029/94JB00039.

Gomberg, J., J. L. Rubinstein, Z. Peng, K. C. Creager, and J. E. Vidale (2008), Widespread triggering of non-volcanic tremor in California, *Science*, *319*, 173, doi:10.1126/science.1149164.

Hanks, T. C., and H. Kanamori (1979), A moment-magnitude scale, *J. Geophys. Res.*, *84*, 2348–2350, doi:10.1029/JB084iB05p02348.

Harris, R. A., and J. R. Arrowsmith (2006), Introduction to the special issue on the 2004 Parkfield earthquake and the Parkfield earthquake prediction experiment, *Bull. Seismol. Soc. Am.*, *96*, S1–S10, doi:10.1785/0120050831.

Hart, R. H. G., M. T. Gladwin, R. L. Gwyther, D. C. Agnew, and F. K. Wyatt (1996), Tidal calibration of borehole strain meters; removing the effects of small-scale inhomogeneity, *J. Geophys. Res.*, *101*, 25,553–25,571, doi:10.1029/96JB02273.

Hill, D. P., and S. G. Prejean (2007), Dynamic triggering in earthquake seismology, in *Treatise on Geophysics*, vol. 4 *Earthquake Seismology*, edited by H. Kanamori, pp. 257–292, Elsevier, New York.

Ide, S., K. Imanishi, Y. Yoshida, G. C. Beroza, and D. R. Shelly (2008), Bridging the gap between seismically and geodetically detected slow earthquakes, *Geophys. Res. Lett.*, *35*, L10305, doi:10.1029/2008GL034014.

Johanson, I. A., and R. Bürgmann (2005), Creep and quakes on the northern transition zone of the San Andreas fault from GPS and InSAR data, *Geophys. Res. Lett.*, *32*, L14306, doi:10.1029/2005GL023150.

Johnston, M. J. S., A. T. Linde, M. T. Gladwin, and R. D. Borcherdt (1987), Fault failure with moderate earthquakes, *Tectonophysics*, *144*, 189–206, doi:10.1016/0040-1951(87)90017-5.

Johnston, M. J. S., G. D. Myren, R. J. Mueller, A. T. Linde, and M. T. Gladwin (1992), A focused earthquake prediction experiment on the southern Hayward fault: Detection array and expected strains and displacements during fault rupture, in *Proceedings of the 2nd Conference on Earthquake Hazards in the Eastern San Francisco Bay Area*, edited by G. Borchardt et al., *Calif. Div. Mines Geol. Spec. Publ.*, *113*, 197–206.

Johnston, M. J. S., R. D. Borcherdt, A. T. Linde, and M. T. Gladwin (2006), Continuous borehole strainmeter and pore pressure in the near field of the 28 September 2004 M6.0 Parkfield, California, earthquake: Implications for nucleation, fault response, earthquake prediction, and tremor, *Bull. Seismol. Soc. Am.*, *96*, S56–S72, doi:10.1785/0120050822.

Kanamori, H., and E. E. Brodsky (2004), The physics of earthquakes, *Rep. Prog. Phys.*, *67*, 1429–1496, doi:10.1088/0034-4885/67/8/R03.

Langbein, J. (2004), Noise in two-color electronic distance meter measurements revisited, *J. Geophys. Res.*, *109*, B04406, doi:10.1029/2003JB002819.

Langbein, J., R. L. Gwyther, R. H. G. Hart, and M. T. Gladwin (1999), Slip-rate increase at Parkfield in 1993 detected by high-precision EDM and borehole tensor strainmeters, *Geophys. Res. Lett.*, *26*, 2529–2532, doi:10.1029/1999GL900557.

Langbein, J., J. R. Murray, and H. A. Snyder (2006), Coseismic and initial postseismic deformation from the 2004 Parkfield, California earthquake, observed by Global Positioning System, electronic distance meter, creepmeters, and borehole strainmeters, *Bull. Seismol. Soc. Am.*, *96*, S304–S320, doi:10.1785/0120050823.

Linde, A. T., M. T. Gladwin, M. J. S. Johnston, R. L. Gwyther, and R. G. Bilham (1996), A slow earthquake sequence on the San Andreas Fault, *Nature*, *383*, 65–68, doi:10.1038/383065a0.

Liu, Y., and J. R. Rice (2007), Spontaneous and triggered aseismic deformation transients in a subduction fault model, *J. Geophys. Res.*, *112*, B09404, doi:10.1029/2007JB004930.

Marone, C., and C. H. Scholz (1988), The depth of seismic faulting and the upper transition from stable to unstable slip regimes, *Geophys. Res. Lett.*, *15*, 621–624, doi:10.1029/GL015i006p00621.

McGill, S. F., C. R. Allen, K. W. Hudnut, D. C. Johnson, W. F. Miller, and K. E. Sieh (1989), Slip on the Superstition Hills Fault and on nearby faults associated with the 24 November 1987 Elmore Ranch and Superstition Hills earthquakes, southern California, *Bull. Seismol. Soc. Am.*, *79*, 362–375.

Nadeau, R. M., and D. Dolenc (2005), Nonvolcanic tremors deep beneath the San Andreas Fault, *Science*, *307*, 389, doi:10.1126/science.1107142.

Okada, Y. (1992), Internal deformation due to shear and tensile faults in a half-space, *Bull. Seismol. Soc. Am.*, *82*, 1018–1040.

Peng, Z., J. E. Vidale, A. G. Wech, R. M. Nadeau, and K. C. Creager (2009), Remote triggering of tremor along the San Andreas Fault in central California, *J. Geophys. Res.*, *114*, B00A06, doi:10.1029/2008JB006049.

Pollitz, F. F., and M. J. S. Johnston (2006), Direct test of static stress versus dynamic stress triggering of aftershocks, *Geophys. Res. Lett.*, *33*, L15318, doi:10.1029/2006GL026764.

Rogers, G., and H. Dragert (2003), Episodic tremor and slip on the Cascadia subduction zone: The chatter of silent slip, *Science*, *300*, 1942–1943, doi:10.1126/science.1084783.

Rubinstein, J. L., J. E. Vidale, J. Gomberg, P. Bodin, K. C. Creager, and S. Malone (2007), Non-volcanic tremor driven by large transient shear stresses, *Nature*, *448*, 579–582, doi:10.1038/nature06017.

Rubinstein, J. L., J. Gomberg, J. E. Vidale, A. G. Wech, H. Kao, K. C. Creager, and G. Rogers (2009), Seismic wave triggering of nonvolcanic tremor, episodic tremor and slip, and earthquakes on Vancouver Island, *J. Geophys. Res.*, *114*, B00A01, doi:10.1029/2008JB005875.

Schmidt, D. A., R. Bürgmann, R. M. Nadeau, and M. d'Alessio (2005), Distribution of aseismic slip rate on the Hayward fault inferred from seismic and geodetic data, *J. Geophys. Res.*, *110*, B08406, doi:10.1029/2004JB003397.

Schwartz, S. Y., and J. M. Rokosky (2007), Slow slip events and seismic tremor at circum-Pacific subduction zones, *Rev. Geophys.*, *45*, RG3004, doi:10.1029/2006RG000208.

Tamura, Y., T. Sato, M. Ote, and M. Ishiguro (1991), A procedure for tidal analysis with a Bayesian information criterion, *Geophys. J. Int.*, *104*, 507–516, doi:10.1111/j.1365-246X.1991.tb05697.x.

Titus, S. J., C. DeMets, and B. Tikoff (2006), Thirty-five year creep rates for the creeping segment of the San Andreas fault and the effects of the 2004 Parkfield earthquake: Constraints from alignment arrays, continuous Global Positioning System and creepmeters, *Bull. Seismol. Soc. Am.*, *96*, S250–S268, doi:10.1785/0120050811.

Wells, D. L., and K. J. Coppersmith (1994), New empirical relationships among magnitude, rupture length, rupture width, rupture area, and surface displacement, *Bull. Seismol. Soc. Am.*, *84*, 974–1002.

J. Gomberg and E. F. Smith, U.S. Geological Survey, Department of Earth and Space Sciences, University of Washington, Box 351310, Seattle, WA 98195-1310, USA. (gomberg@usgs.gov)